A CONSTITUTIVE MODEL AND DATA FOR METALS SUBJECTED TO LARGE STRAINS, HIGH STRAIN RATES AND HIGH TEMPERATURES

Gordon R. Johnson
Honeywell Inc.
Defense Systems Division
Hopkins, Minesota 55343 USA

William H. Cook
Air Force Armament Laboratory
Eglin Air Force Base, Florida 32542 USA

This paper presents a constitutive model and data for materials subjected to large strains, high strain rates and high temperatures. The basic form of the model is well suited for computations because it uses variables which are readily available in most of the applicable computer codes. The materials considered are OFHC copper, Cartridge brass, Nickel 200, Armco iron, Carpenter electrical iron, 1006 steel, 2024-T351 aluminum, 7039 aluminum, 4340 steel, S-7 tool steel, Tungsten alloy and DU-.75Ti (depleted uranium). The data for the material constants are obtained from torsion tests over a wide range of strain rates, static tensile tests, dynamic Hopkinson bar tensile tests and Hopkinson bar tests at elevated temperatures. The model and data are evaluated by comparing computational results with data from cylinder impact tests.

INTRODUCTION

During recent years there has been a great deal of effort directed at computations for intense impulsive loading due to high-velocity impact and explosive detonation. The capabilities of current computer codes have been extended to the point that the limiting factor is often that of adequately defining material characteristics for both strength and fracture. A common approach is to simply repeat the computations with different material characteristics until agreement with experiment is obtained. Clearly it would be desirable to be able to characterize materials with a limited number of laboratory tests so the initial computations could be used with more confidence. This would result in a more efficient design cycle and would also give increased insight into understanding the complicated processes which occur during intense impulsive loading conditions.

This paper presents a constitutive model which is primarily intended for computations. It is recognized that more complicated models may indeed give more accurate descriptions of material behavior. Similarly, various models may give better descriptions for various materials. In many instances, however, the computational user cannot readily incorporate complicated and diverse models. The result is that a constant "dynamic flow stress" is often used.

In the following sections test data will be presented and the approach used to extract the appropriate material constants from the data will be explained. This will be done in detail for three materials (OFHC copper, Armco iron and 4340 steel). Results for the other nine materials will be included, but with limited discussion. Finally, the model and data will be evaluated by comparing computational results to data from cylinder impact tests.

TEST DATA

The test data are primarily obtained from torsion tests over a wide range of strain rates (quasi-static to about 400 s^{-1}) and dynamic Hopkinson bar tensile tests over a range of temperatures. Static tensile test data are also used. The specific torsion testing apparatus is described in [1] and a representative Hopkinson bar apparatus is described in [2].

Figure 1 shows Hopkinson bar test data at various temperatures. The elevated temperatures are obtained by surrounding the in-place test specimen by an oven such that the temperatures are applied for several minutes prior to testing. Although it is possible to test materials to greater strains than those shown in Figure 1, the Hopkinson bar data cannot be accurately evaluated after necking begins to occur in the tensile specimens. Futhermore, at large strains the effects of adiabatic heating can also complicate the results. The elevated temperatures show a distinct softening effect on the strength of the materials.

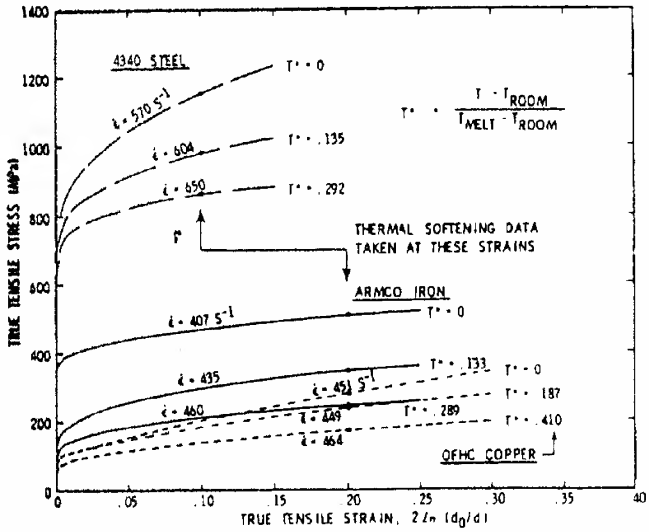

Figure 1. Stress-Strain Data for Hopkinson Bar Tests at Various Temperatures

Torsion data for the same three materials are shown in Figure 2. Comparable data for the other nine materials are presented elsewhere [3,4]. Some desirable features of this testing technique are that the state of stress in the specimen is well defined, large shear strains can be achieved without forming geometric instabilities, and a wide range of strain rates can be obtained with the same testing technique.

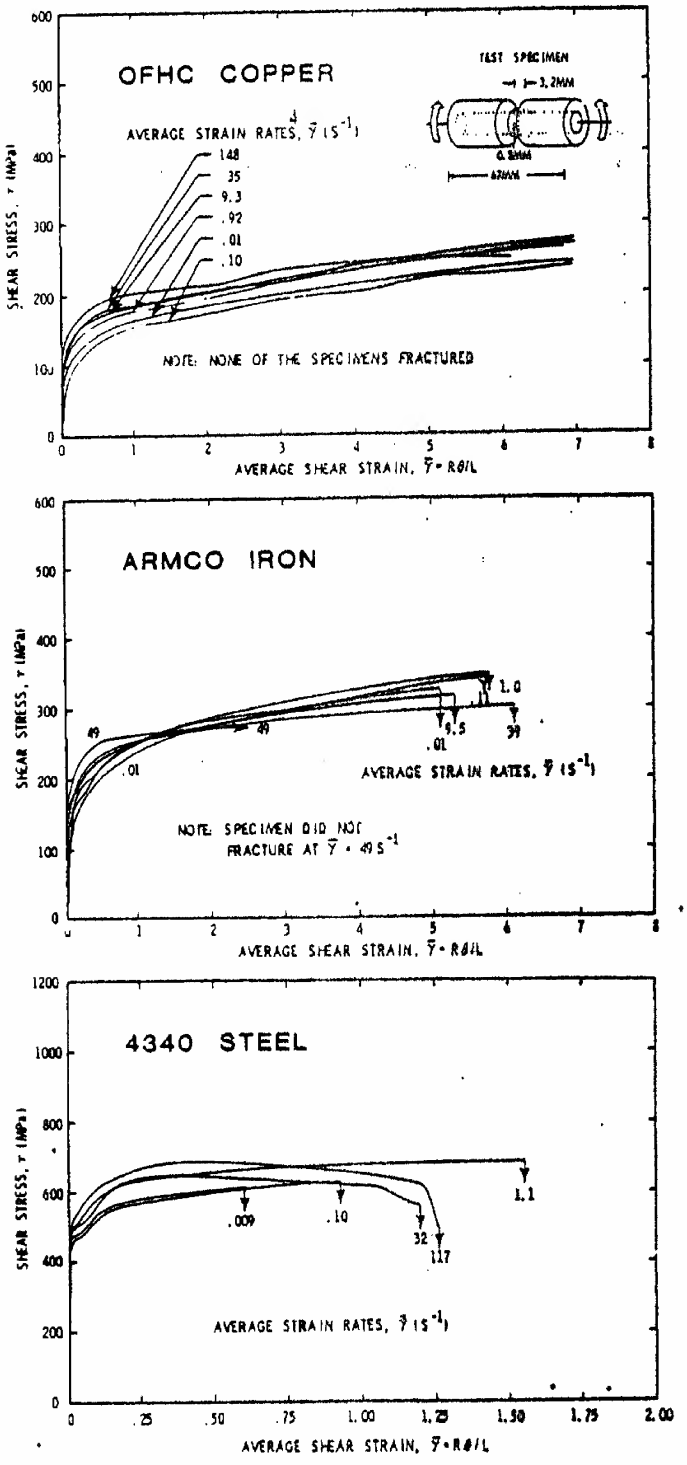

Figure 2. Stress-Strain Data for Torsion Tests at Various Strain Rates

Quasi-static stress-strain data for both tension and torsion tests are shown in Figure 3. An equivalent tensile flow stress is obtained from the torsion data by using the von Mises flow rule; the tensile stress is $\sigma = \sqrt{3}\tau$ and the corresponding tensile strain is $\epsilon = \gamma/\sqrt{3}$.

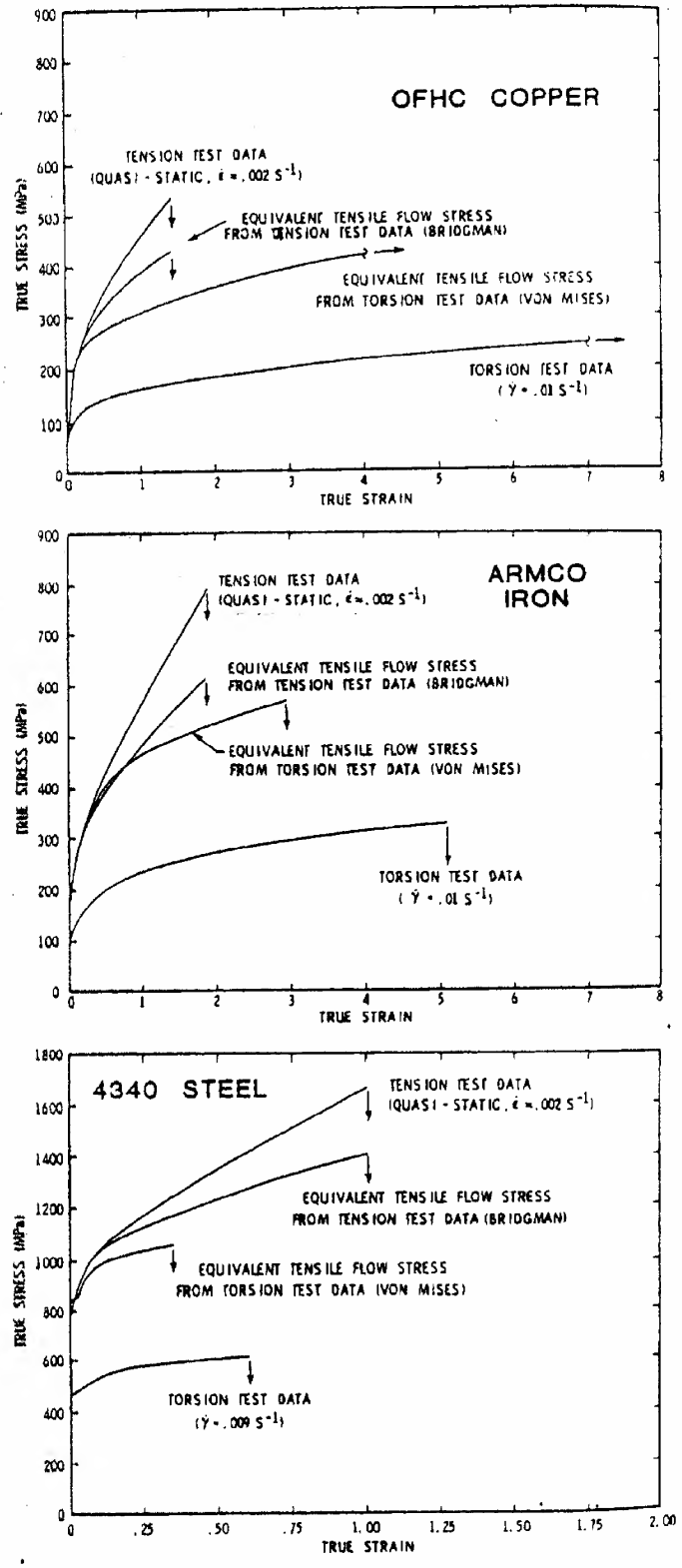

Figure 3. Comparison of Quasi-Static Stress-Strain Data for Tension and Torsion Tests

The stress for the tension test data is based on the current area of the neck, and the strain is defined as $\ln (A_o/A)$, where A_o and A represent the initial and current areas of the neck.

At larger strains, after necking has begun, the net tensile stress is greater than the tensile flow stress. This is due to the presence of hydrostatic tension. The equivalent tensile flow stress, obtained from the tension data, is approximately determined by using the Bridgman correction factor [5].

In all three instances the tension data tend to indicate a higher strength than that derived from the torsion data. Therefore, it is desirable to have data from both tension and torsion tests such that the discrepancy between the two modes of deformation can be identified and compensated.

Figures 4 and 5 show the effect of strain rate for both torsion and tension. Comparable torsion data for the other materials are given in [3] and [4]. In all instances the stress increases as the strain rate increases.

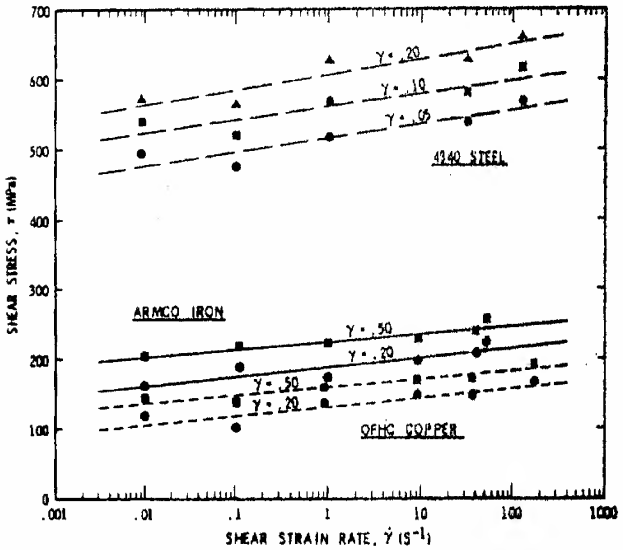

Figure 4. Stress vs Strain Rate for the Torsion Tests

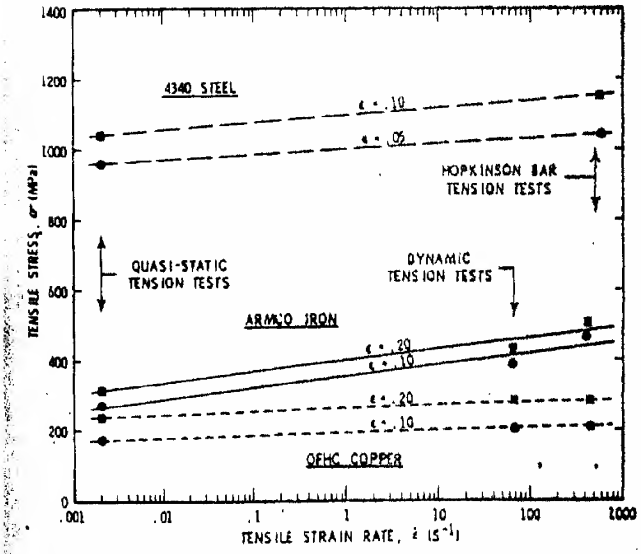

Figure 5. Stress vs Strain Rate for the Tension Tests

DATA ANALYSIS AND MODEL DEVELOPMENT

The model for the von Mises flow stress, σ, is expressed as

$$\sigma = [A + B\,\epsilon^n]\,[1 + C \ln \dot{\epsilon}^*]\,[1 - T^{*m}]$$

where ϵ is the equivalent plastic strain, $\dot{\epsilon}^* = \dot{\epsilon}/\dot{\epsilon}_o$ is the dimensionless plastic strain rate for $\dot{\epsilon}_o = 1.0\ s^{-1}$ and T^* is the homologous temperature. The five material constants are A, B, n, C, m. The expression in the first set of brackets gives the stress as a function of strain for $\dot{\epsilon}^* = 1.0$ and $T^* = 0$. The expressions in the second and third sets of brackets represent the effects of strain rate and temperature, respectively. The basic form of the model is readily adaptable to most computer codes since it uses variables (ϵ, $\dot{\epsilon}^*$, T^*) which are available in the codes.

The first step in the process is to determine the constants in the first set of brackets. A is the yield stress and B and n represent the effects of strain hardening. Since the torsion data include the strain rate of interest ($\dot{\epsilon}^* = 1.0$), it is a straightforward procedure to obtain the appropriate constants for this strain rate. However, these constants are for isothermal conditions ($T^* = 0$) so the effects of adiabatic heating must be considered in analyzing the torsion data [3,4].

The same three constants can also be derived from the tension data. Here the starting point is the equivalent tensile flow stress from the tension data, as shown in Figure 3. This approximate flow stress, obtained by using the Bridgman correction factor, is adjusted based on finite element simulations of the tension test. The proper flow stress will give computed results which agree with the tension test data of Figure 3. Generally, the Bridgman correction factor gives acceptable results, and the adjustments due to the refining computations are not large.

The flow stress which is eventually determined from the quasi-static tension test is for $\dot{\epsilon}^* = 0.002$ and must therefore be adjusted for $\dot{\epsilon}^* = 1.0$. This is done by increasing the quasi-static values of the constants A and B, by the ratio of the stresses at $\dot{\epsilon}^* = 1.0$ and $\dot{\epsilon}^* = 0.002$, as shown in Figure 5.

The preceding gives two sets of constants, one for torsion and one for tension. For general computational purposes, the average values of A, B and n can be used. The resulting adiabatic flow stress, based on average values of the constants, is generally within about 10 percent of that obtained by using either the torsion or the tension data.

The effect of thermal softening is shown in Figure 6. The thermal softening fraction, K_T, is simply the ratio of the stress at elevated temperature to that at room temperature. The data are taken from the Hopkinson bar tests of Figure 1. The Armco iron is shown to soften very rapidly with increasing temperature, and this is in close agreement with static data [3,6]. The OFHC copper shows an approximately linear dependence on T^*. This is not in good agreement

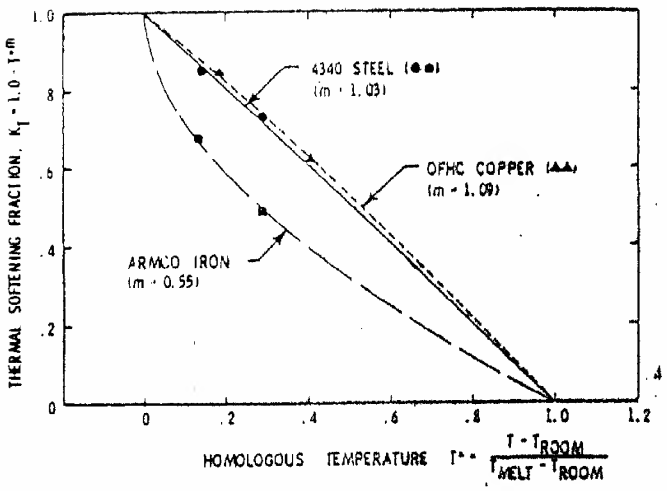

Figure 6. Thermal Softening Fraction vs Temperature for the Hopkinson Bar Tests

with static data [3,7], which tend to soften more rapidly as T* increases. There is some evidence, however, that the thermal softening fraction tends to increase as the strain rate increases [8]. This trend is consistent with the results reported herein.

The strain rate constant, C, is determined next. For the tensile mode of deformation it can be obtained from the data of Figure 5. Similarly, for torsion it can be obtained from the data of Figure 4. The torsion data also allow the combination of the strain rate hardening and thermal softening to be evaluated at large strains. This is done by numerically simulating the torsion test at high strain rates. Strain hardening, strain rate hardening, thermal softening and heat conduction effects are considered [9]. In some instances the strain rate constant is adjusted to give better agreement with torsion test data at large strains. Figure 7 shows a comparison of the computed and test results using the torsional strain rate constants. The final strain rate constant is taken as an average of those obtained from the tensile data and the torsion data.

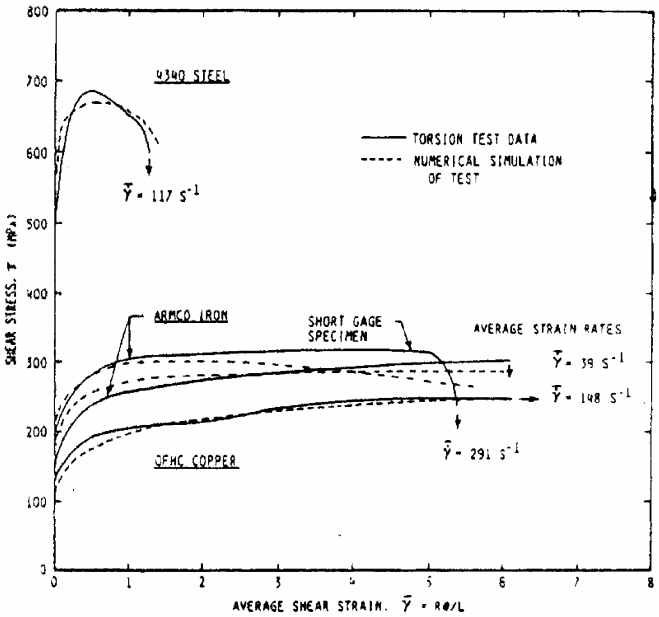

Figure 7. Comparison of Test Data and Numerical Simulations for the Highest Strain Rate Torsion Tests

The resulting constants for the 12 materials are presented in Table 1. The corresponding stress-strain relationships are shown in Figure 8. The temperature for

Table 1. Constitutive Constants for the Various Materials

MATERIAL	DESCRIPTION				CONSTITUTIVE CONSTANTS FOR $\sigma = [A + B\epsilon^n][1 + C\ln\dot{\epsilon}^*][1 - T^{*m}]$				
	HARDNESS (ROCKWELL)	DENSITY (Kg/m³)	SPECIFIC HEAT (J/KgK)	MELTING TEMPERATURE (K)	A (MPa)	B (MPa)	n	C	m
OFHC COPPER	F-30	8960	383	1356	90	292	.31	.025	1.09
CARTRIDGE BRASS	F-67	8520	385	1189	112	505	.42	.009	1.68
NICKEL 200	F-79	8900	446	1726	163	648	.33	.006	1.44
ARMCO IRON	F-72	7890	452	1811	175	380	.32	.060	0.55
CARPENTER ELECTRICAL IRON	F-83	7890	452	1811	290	339	.40	.055	0.55
1006 STEEL	F-94	7890	452	1811	350	275	.36	.022	1.00
2024-T351 ALUMINUM	B-75	2770	875	775	265	426	.34	.015	1.00
7039 ALUMINUM	B-76	2770	875	877	337	343	.41	.010	1.00
4340 STEEL	C-30	7830	477	1793	792	510	.26	.014	1.03
S-7 TOOL STEEL	C-50	7750	477	1763	1539	477	.18	.012	1.00
TUNGSTEN ALLOY(.07Ni, .03Fe)	C-47	17000	134	1723	1506	177	.12	.016	1.00
DU-.75Ti	C-45	18600	117	1473	1079	1120	.25	.007	1.00

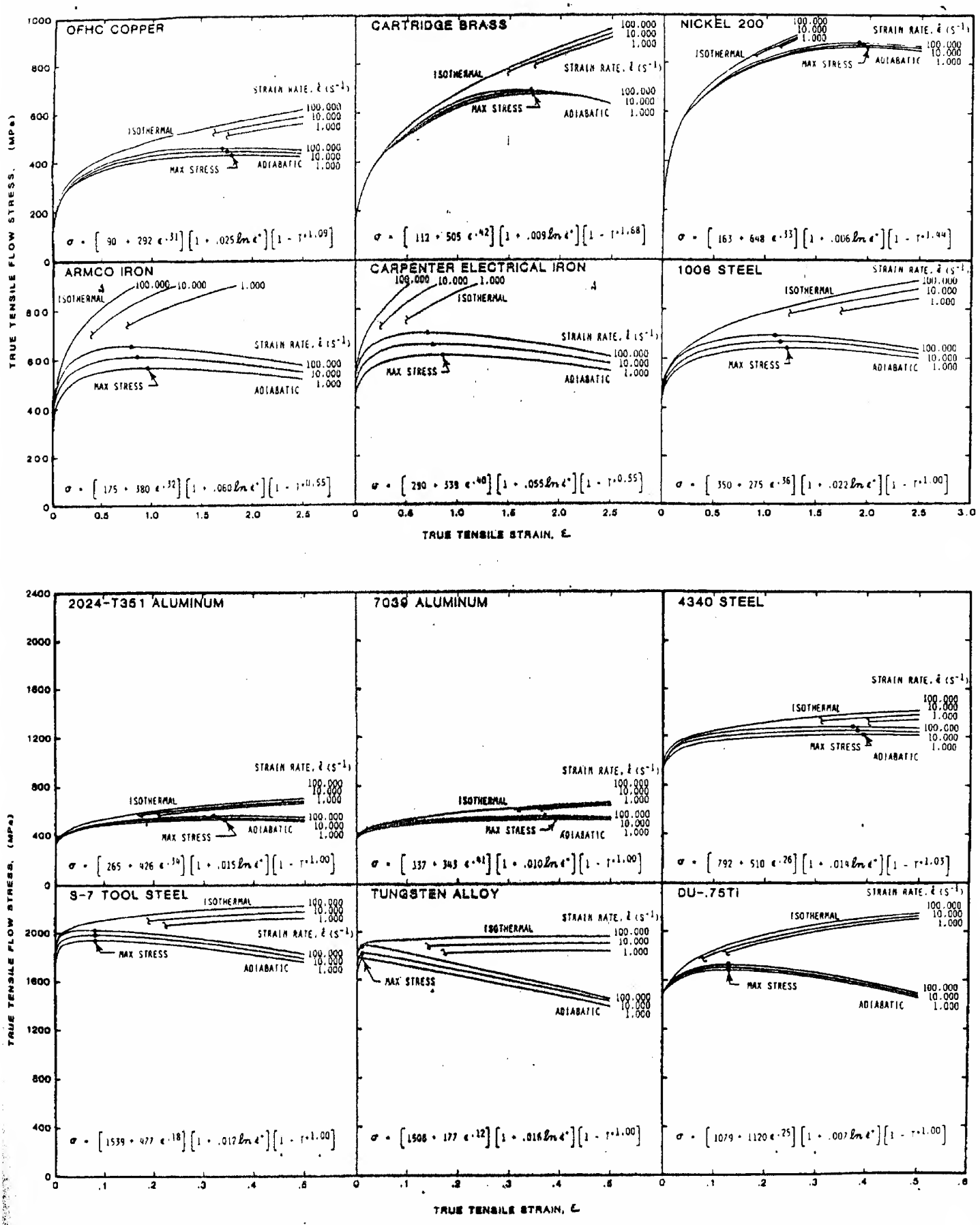

Figure 8. Isothermal and Adiabatic Stress-Strain Relationships for the Various Materials

the adiabatic relationships is due to the plastic work of deformation. In all cases, the adiabatic stresses reach a maximum and then decrease with increasing strain. The point of maximum stress is important inasmuch as it represents the strain at which localized instabilities may begin to occur.

Some comments should be made about the materials other than the OFHC copper, Armco iron and 4340 steel. The Cartridge brass and Nickel 200 have several similarities; they are not very sensitive to strain rate [3], the flow stress derived from the tensile data is significantly greater than that obtained from the torsion data [3], and the thermal softening is less pronounced than for the other materials. The thermal softening data obtained from the Hopkinson bar tests gives m = 1.68 (Cartridge brass) and m = 1.44 (Nickel 200). This is consistent with static data [3,10, 11].

No Hopkinson bar tests were performed on the Carpenter electrical iron and it is assumed that its thermal softening characteristics are similar to that of the Armco iron. Hopkinson bar tests were performed on the 1006 steel and some very unexpected results were obtained. At lower temperatures ($0 < T^* < .2$) the thermal softening data are similar to that of the Armco iron. At higher temperatures, however, ($.2 < T^* < .4$) K_T increases sharply as the temperature increases. Since these results cannot be adequately explained, the thermal softening fraction is assumed to vary in a linear manner (m = 1.00). The other constants for the 1006 steel are obtained from the torsion data only [3].

The data for the remaining materials (2024-T351 aluminum, 7039 aluminum, S-7 tool steel, Tungsten alloy and DU-.75Ti) are also obtained from torsion data only [4]. No tensile data are included. The thermal softening fraction is again assumed to vary in a linear manner.

EVALUATION WITH CYLINDER IMPACT TESTS

An evaluation of the model and data can be made by comparing computed results with data from cylinder impact tests. These tests provide strain rates in excess of 10^5 s^{-1} and strains in excess of 2.0. Also, a range of tensile and shear deformations is experienced.

The results of these comparisons are shown in Figure 9. The computations were performed with the EPIC-2 code. For these computations an average pressure was used for each set of adjacent triangular elements such that the excessive stiffness sometimes associated with triangular elements is essentially eliminated [12]. The Armco iron and 4340 steel show very good agreement. The OFHC copper results do not agree as well, but even these are acceptable for most applications. It should be emphasized that the results of cylinder impact tests have not been incorporated into the data, and they represent a totally independent check case. Photographs of the impacted cylinders are shown in Figure 10.

SUMMARY AND CONCLUSIONS

A computational model for flow stress has been presented which includes the effects of strain hardening, strain rate hardening and thermal softening. Some well-defined laboratory tests have been performed on 12 materials to obtain data for this model. An independent evaluation has shown the model and data to give good computational results for a range of cylinder impact conditions.

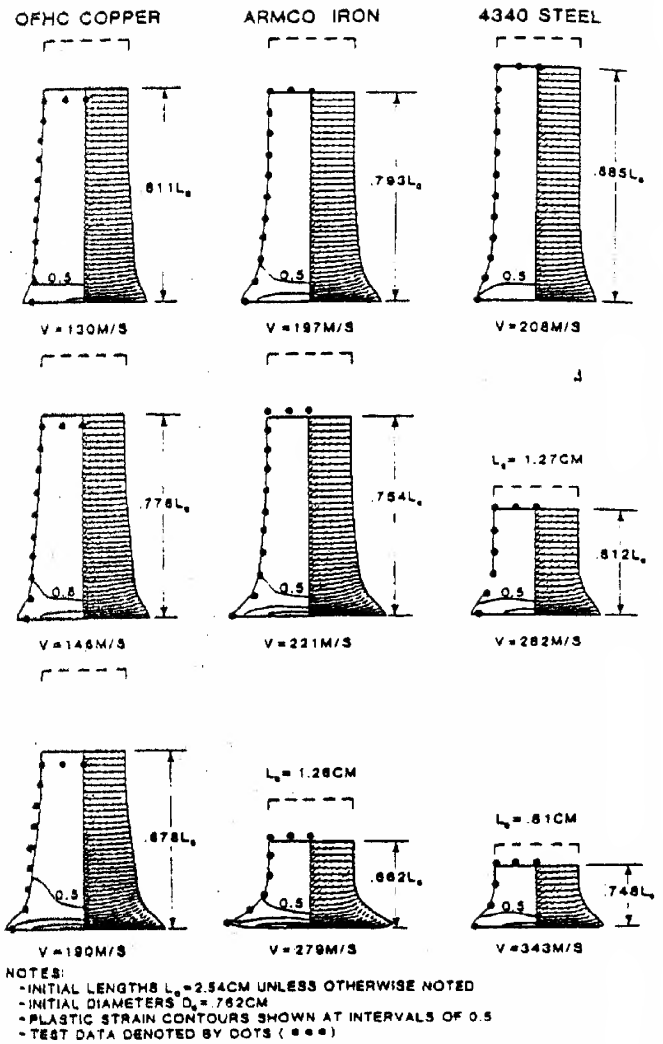

Figure 9. Comparison of Computed Shapes and Test Results for Cylinder Impact Tests at Various Velocities

ACKNOWLEDGEMENTS

This work was funded by Contract F08635-81-C-0179 from the U.S. Air Force and a Honeywell Independent Development Program.

REFERENCES

1. Lindholm, U.S., Nagy. A., Johnson, G.R., and Hoegfeldt, J.M, "Large Strain, High Strain Rate Testing of Copper," ASME **Journal of Engineering Materials and Technology**, Vol. 102, No. 4, October 1980.

2. Nicholas, T., "Tensile Testing of Materials at High Rates of Strain," **Experimental Mechanics**, May 1981.

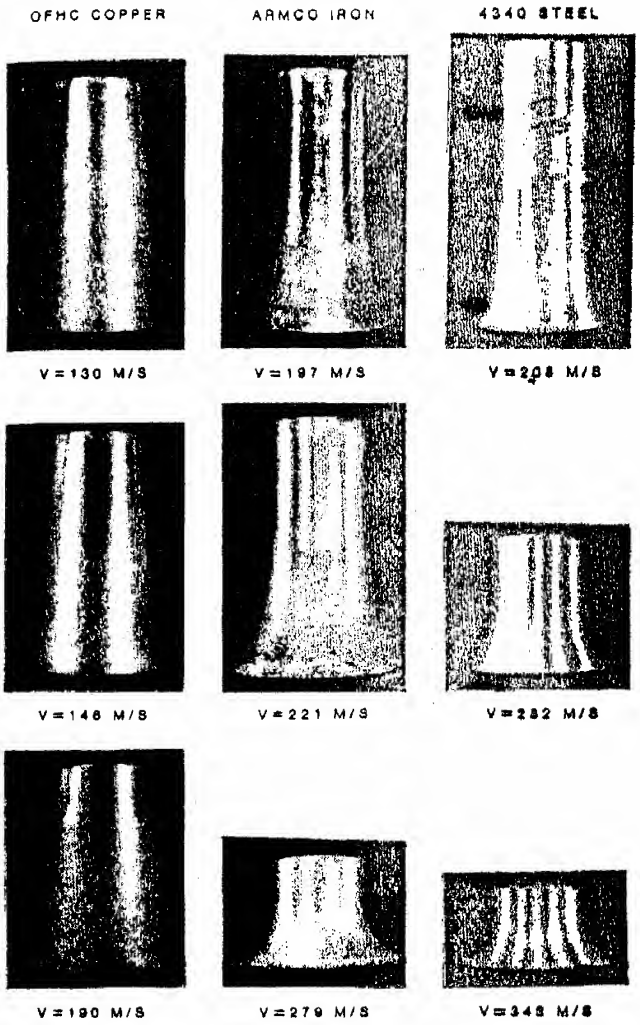

Figure 10. Photographs of the Impacted Cylinders

3. Johnson, G.R., Hoegfeldt, J.M., Lindholm, U.S., and Nagy, A., "Response of Various Metals to Large Torsional Strains over a Large Range of Strain Rates — Part 1: Ductile Metals," ASME **Journal of Engineering Materials and Technology**, Vol. 105, No. 1, January 1983.

4. Johnson, G.R., Hoegfeldt, J.M., Lindholm, U.S., and Nagy, A., "Response of Various Metals to Large Torsional Strains over a Large Range of Strain Rates — Part 2: Less Ductile Metals," ASME **Journal of Engineering Materials and Technology**, Vol. 105, No. 1, January 1983.

5. Bridgman, P.W., **Studies in Large Plastic Flow and Fracture**, McGraw-Hill, 1952.

6. Leslie, W.C., "Iron and Its Dilute Substitutional Solid Solutions," **Metallurgical Transactions**, Vol. 3, January 1972.

7. Hawkyard, J.B., Eaton, D., and Johnson, W., "The Mean Dynamic Yield Strength of Copper and Low Carbon Steel at Elevated Temperatures from Measurments of the Mushrooming of Flat-Ended Projectiles," **International Journal of Mechanical Sciences**, Vol. 10, No. 12, 1968.

8. Nadai, A., and Manjoine, M.J., "High Speed Tension Tests at Elevated Temperatures — Parts II and III," Journal of **Applied Mechanics**, Vol. 8, June 1941.

9. Johnson, G.R., "Dynamic Analysis of a Torsion Test Specimen Including Heat Conduction and Plastic Flow," ASME **Journal of Engineering Materials and Technology**, Vol. 103, No. 3, July 1981.

10. Izumi, O., and Harada, Y., "Repeated Yielding and Abnormal Hardening in High-Temperature and Tensile Deformation of α-Brass," Trans. **Japan Institute of Metals**, Vol. 11, 1970.

11. Huntington Nickel Alloys Bulletin.

12. Johnson, G.R., "Recent Developments and Analyses Associated with the EPIC-2 and EPIC-3 Codes," ASME **1981 Advances in Aerospace Structures and Materials**, AD-01, Wang, S.S. and Renton, W.J. eds., 1981.